Rapid Communications

"Container" evolution for cluster structures in ^{16}O

Y. Funaki

College of Science and Engineering, Kanto Gakuin University, Yokohama 236-8501, Japan;
School of Physics and Nuclear Energy Engineering and IRCNPC, Beihang University, Beijing 100191, China;
and Nishina Center for Accelerator-Based Science, RIKEN, Wako 351-0198, Japan

(Received 4 January 2018; published 22 February 2018)

Background: $\alpha + {}^{12}$C clustering in ^{16}O has been of historical importance in nuclear clustering. In the last 15 years the 4α condensate state has been proposed as a new-type cluster state.
Purpose: The aim is to reveal a dynamical process of the formation of different kinds of cluster states, in terms of a "container" aspect of clusters, in ^{16}O.
Method: The so-called THSR wave function for the 4α clusters is extended to inclusion of two different "containers" occupied independently by the ^{12}C (3α) and α clusters.
Results: The five $J^\pi = 0^+$ states with 4α tetrahedral shape, $\alpha + {}^{12}$C cluster structures, and the 4α condensate character, are found to be represented, to good approximation, by single configurations of the extended THSR wave function with "containers" of appropriate shape and size.
Conclusions: It is demonstrated in ^{16}O that the dynamical evolution of cluster structures can be caused by size and shape evolution of a "container" occupied with clusters. The α condensate with gaslike 4α configuration appears as a limit of the cluster formation.

DOI: 10.1103/PhysRevC.97.021304

Alpha-like four-nucleon correlation plays an important role in nuclei, in which spin and isospin are saturated. In particular, $A = 4n$ ($N = Z$) light nuclei tend to have α cluster structures in their excited states. The 3α cluster structure in ^{12}C, $\alpha + {}^{12}$C cluster structure in ^{16}O, and $\alpha + {}^{16}$O cluster structure in ^{20}Ne are typical examples and their realities are firmly established in many historical works [1].

In the past 15 years, α-particle condensate structure has been extensively studied theoretically and experimentally. Although providing direct observatory evidence is still in an open question [2–4], many theoretical calculations predict the existence of the 3α and 4α condensate states in ^{12}C and ^{16}O, respectively, in which all α clusters weakly interact with each other with a dilute gaslike configuration, and occupy an identical orbit of a mean-field-like potential [5–10].

On the other hand, the ordinary non-gaslike cluster states like the $\alpha + {}^{16}$O, $\alpha + {}^{12}$C inversion doublets, linear-chain α-cluster states, etc., are completely different from the gaslike cluster states. They had been understood by a concept of localized clustering, in which all clusters are in a geometric arrangement. However, more recent works have required us to modify the basic idea of understanding the ordinary cluster states. The authors in Ref. [11] introduced a microscopic $\alpha + {}^{16}$O cluster model wave function, which demonstrates a nonlocalized motion of the α and ^{16}O clusters. They proved that the model wave function coincides with the full solution of $\alpha + {}^{16}$O RGM equation of motion for all the $\alpha + {}^{16}$O inversion doublet band states. Similar results are also obtained for the 3α and 4α linear-chain states [12], which are originally proposed by Morinaga [13]. All these results lead to the idea that dynamically mutual clusters are confined in a "container," whose shape and size are flexibly conformed, in a nonlocalized way. This new concept of the so-called "container" picture modifies the preceding understanding of nuclear clustering, because the localized clustering has been an important basis to understand the ordinary (non-gaslike) nuclear cluster structures.

In this Rapid Communication, I discuss the nuclear clustering in ^{16}O, because this is a typical nucleus of gaslike and non-gaslike cluster states coexisting. The special interest is in how both gaslike and non-gaslike cluster states, which seem to be quite different from each other, are successively formed as the increase of excitation energy. The $\alpha + {}^{12}$C cluster structure in ^{16}O is formed by the activation of cluster degree of freedom in the ground state having a dual property [14–16], i.e., by the excitation of relative motion between the α and ^{12}C clusters. The gaslike 4α cluster state is then produced as a result of further excitation of the ^{12}C core, to the 3α cluster state, i.e., to the Hoyle state [3]. The path of this cluster evolution is shown in the famous Ikeda diagram, together with many other paths in many other nuclei [17]. I show that this path of cluster evolution along the excitation energy in ^{16}O is nothing but the path of a size and shape evolution of a "container," which provides a new framework of describing both gaslike and non-gaslike cluster states simultaneously.

I adopt a model wave function to realize the above mentioned picture, which is the extended version of the so-called THSR wave function (eTHSR). It is given by a natural extension of what are used in many previous works of ^{8}Be [18], ^{12}C [5,6,19–22], ^{16}O [23], ^{20}Ne [11], ^{9}Be [24] and ^{10}Be [25], ${}^{9}_{\Lambda}$Be [26], ${}^{13}_{\Lambda}$C [27], etc., and has the following

form:

$$\Phi(\boldsymbol{\beta}_1,\boldsymbol{\beta}_2)=\mathcal{A}\left[\exp\left\{-\sum_k^{x,y,z}\frac{1}{2B_{1k}^2}\left(\mu_1\xi_{1k}^2+\mu_2\xi_{2k}^2\right)\right\}\phi_1(b)\phi_2(b)\phi_3(b)\exp\left\{-\sum_k^{x,y,z}\frac{1}{2B_{2k}^2}\mu_3\xi_{3k}^2\right\}\phi_4(b)\right], \quad (1)$$

with $\mathcal{A}$ being the antisymmetrization operator acting on the 16 nucleons, $\phi_i(b)$ the internal wave function of the ith α particle assuming a $(0s)^4$ harmonic oscillator configuration with the width parameter b. $\boldsymbol{\xi}_i$ is the Jacobi coordinates between the α particles, and $\mu_i=4i/(i+1)$, for $i=1,2,3$. While the parameter b characterizes the size of the constituent α particle, the parameters $\boldsymbol{B}_1$ and $\boldsymbol{B}_2$ characterize the size and shape of a "container," in which the α clusters are confined. I can instead define parameters β_{jk} that satisfy the relation, $B_{jk}^2=b^2+2\beta_{jk}^2$, with $j=1,2$ and $k=x,y,z$. However, throughout this study, I assume the axial symmetry $\beta_{i\perp}\equiv\beta_{ix}=\beta_{iy}$, so as to deal with the four parameters, $\beta_{1\perp},\beta_{1z},\beta_{2\perp},\beta_{2z}$, in the practical calculations.

The exponential functions in Eq. (1) represent the center-of-mass (c.m.) motions of the α clusters, in terms of the corresponding Jacobi coordinates. If the $\boldsymbol{B}_1$ and $\boldsymbol{B}_2$ take a common value, i.e., $\boldsymbol{B}_1=\boldsymbol{B}_2=\boldsymbol{B}$, then Eq. (1) results in the following original THSR wave function, in which all α clusters occupy an identical orbit,

$$\Phi(\boldsymbol{\beta})=\mathcal{A}\left[\prod_{i=1}^{4}\exp\left\{-2\sum_k^{x,y,z}(R_{ik}-X_{Gk})^2/B_k^2\right\}\phi(\alpha_i)\right], \quad (2)$$

with $\boldsymbol{R}_i$ the position vector of the ith α cluster and $\boldsymbol{X}_G$ the total c.m. coordinate. This is the α condensate state in a "gas" phase if the magnitude of the parameter $|\boldsymbol{B}|$ is large enough for the antisymmetrizer $\mathcal{A}$ to be negligible [28]. On the contrary, when $|\boldsymbol{B}|\to b$, i.e., $\boldsymbol{\beta}\to 0$, the normalized THSR wave function coincides with the shell-model wave function [10].

We should note that the way of describing cluster states in this model wave function is completely different from those in other traditional cluster models, like the Brink-Bloch wave function [29] and even the antisymmetrized molecular dynamics (AMD) wave function [30], in which clusters are spatially positioned in a localized way, to form a multicentered Slater determinant. In the present model, constituent clusters are arranged without mutually forming any geometric rigid-shaped configuration. This wave function is then far away from the single multicentered Slater determinant and is represented as an infinite number of superpositions of the Slater determinants [10]. A very schematic picture representing the eTHSR wave function in the present ^{16}O system is shown in Fig. 1, in which the 3α clusters and another α cluster are confined in different "containers" characterized by the parameters $\boldsymbol{B}_1$ and $\boldsymbol{B}_2$, respectively. This is contrasted with the Brink-Bloch wave function, in which the cluster configurations are described by their relative distance parameters.

To obtain the energy spectrum, first I impose the so-called r^2-constraint method [21–23,31], to effectively and roughly eliminate spurious continuum components from the present model space. A spurious continuum state is calculated to have a large rms radius in the bound state approximation, and hence this method is to remove the components with extremely large rms radii in the following way,

$$\sum_{\boldsymbol{\beta}_1',\boldsymbol{\beta}_2'}\langle\Phi^{J=0}(\boldsymbol{\beta}_1,\boldsymbol{\beta}_2)|\widehat{\mathcal{O}}_{\rm rms}-\{R^{(\gamma)}\}^2|\Phi^{J=0}(\boldsymbol{\beta}_1',\boldsymbol{\beta}_2')\rangle \times g^{(\gamma)}(\boldsymbol{\beta}_1',\boldsymbol{\beta}_2')=0, \quad (3)$$

with $\widehat{\mathcal{O}}_{\rm rms}=\sum_{i=1}^{16}(\boldsymbol{r}_i-\boldsymbol{X}_G)^2/16$, and $\Phi^{J=0}(\boldsymbol{\beta}_1,\boldsymbol{\beta}_2)=\widehat{P}^{J=0}\Phi(\boldsymbol{\beta}_1,\boldsymbol{\beta}_2)$, where $\widehat{P}^{J=0}$ is the projection operator of angular-momentum $J=0$ and use is made of the notation $\boldsymbol{\beta}_i=(\beta_{i\perp},\beta_{iz})$ with $i=1,2$. The eigenfunctions of the above equation are expressed below,

$$\Phi^{(\gamma)}=\sum_{\boldsymbol{\beta}_1,\boldsymbol{\beta}_2}g^{(\gamma)}(\boldsymbol{\beta}_1,\boldsymbol{\beta}_2)\Phi^{J=0}(\boldsymbol{\beta}_1,\boldsymbol{\beta}_2). \quad (4)$$

I now eliminate the eigenstates with the eigenvalues, $R^{(\gamma)}\geqslant 7.0$ fm, from the following linear combination:

$$\Psi_\lambda=\sum_\gamma f_\lambda^{(\gamma)}\Phi^{(\gamma)}. \quad (5)$$

The coefficients of the above expansion is determined by solving the Hill-Wheeler equation,

$$\sum_{\gamma'}\langle\Phi^{(\gamma)}|H-E_\lambda|\Phi^{(\gamma')}\rangle f_\lambda^{(\gamma')}=0. \quad (6)$$

For Hamiltonian, I adopt the effective nucleon-nucleon interaction with finite range three-body force called F1 force [32]. Note that, for example, if we adopt other forces like Volkov No. 1 and No. 2 [33], no reasonable force parameter is found to reproduce both $\alpha+{}^{12}$C threshold energy and the ground-state energy of ^{16}O [34], while it is shown that the F1 force gives a much better simultaneous description of ^{12}C and ^{16}O [35].

In Fig. 2, the calculated energy spectrum for $J^\pi=0^+$ states is shown. The corresponding experimental data and result by the previous 4α OCM calculation [9] are also shown. The

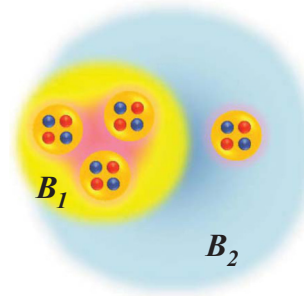

FIG. 1. Schematic representation of the eTHSR wave function, in which the two "containers" of the 3α and α clusters are characterized by the parameters $\boldsymbol{B}_1$ and $\boldsymbol{B}_2$, respectively.

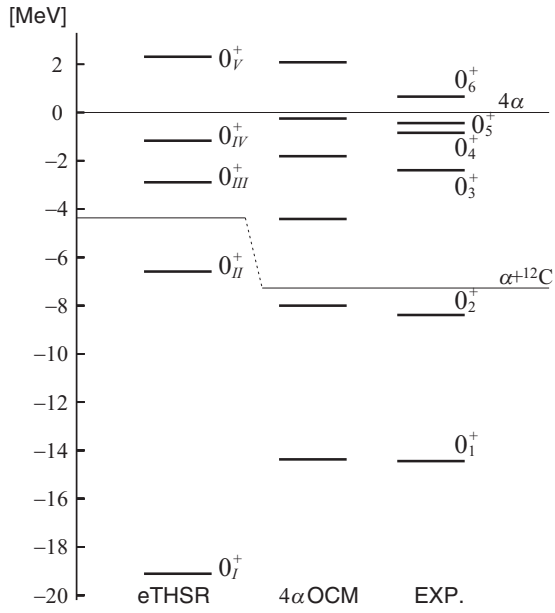

FIG. 2. Energy spectra of the low-lying $J^\pi = 0^+$ states calculated with the extended THSR ansatzes. The corresponding observed spectrum (Expt.) [38,39] and result by the 4α OCM [9] are also shown. The numbers are rms radii in a unit of fm.

solution of the Hill-Wheeler equation with the r^2-constraint method is shown. The 0^+_V state is actually the seventh 0^+ state obtained by solving the Hill-Wheeler equation, i.e., the fifth and sixth eigenstates are kicked out from the present consideration, because they have larger rms radii and are regarded as spurious continuum states accidentally mixed with the physical states.

In the 4α OCM calculation, it is reported that the 0^+_6 state has the 4α condensate character and the $0^+_2 - 0^+_5$ states all have $\alpha + {}^{12}$C cluster structures. i.e., $\alpha(S) + {}^{12}\mathrm{C}(0^+_1)$, $\alpha(D) + {}^{12}\mathrm{C}(2^+_1)$, $\alpha(S) + {}^{12}\mathrm{C}(0^+_1)$, and $\alpha(P) + {}^{12}\mathrm{C}(1^-)$ cluster structures, respectively. The difference between the 0^+_2 and 0^+_4 states are that in the latter the α and ^{12}C relative motion is further excited and has a higher nodal S wave, to have a larger rms radius than the former.

Because in the present eTHSR wave function of Eq. (1) the α clusters occupy positive parity orbits, such a state as having the $\alpha(P) + {}^{12}\mathrm{C}(1^-)$ cluster structure, like the 0^+_5 state in the OCM calculation, is missing. The inclusion of negative parity orbit in the THSR ansatz is also possible and will be shown in the forthcoming paper. I mention that in fact an extension to such a direction is already done [11,24,25]. However, for the other states, a one-to-one correspondence to the experimental data as well as to the 4α OCM calculation is consistently obtained. It should be noted that in the OCM calculations [9,36,37], the binding energies of the ground states of ^{16}O and the ^{12}C are phenomenologically fitted to the corresponding experimental values. In the present calculation, however, there is no adjustable parameter in the microscopic Hamiltonian.

In Table I, rms radii and monopole matrix elements with the ground state are shown. The experimental data available are reasonably reproduced. We can also see that from the 0^+_I to

TABLE I. rms charge radii and monopole matrix elements of the $0^+_I - 0^+_V$ states calculated with the eTHSR ansatz, in comparison with the corresponding experimental data.

	eTHSR		Expt.	
	$R_{\rm rms}$ (fm)	$M(E0)\,(e\mathrm{fm}^2)$	$R_{\rm rms}$ (fm)	$M(E0)\,(e\mathrm{fm}^2)$
0^+_I	2.7		2.71(0.02)	
0^+_{II}	3.2	5.9		3.55(0.21)
0^+_{III}	3.3	5.7		4.03(0.09)
0^+_{IV}	4.9	0.8		
0^+_V	4.9	0.7		

the 0^+_V states, i.e., as the states are excited, the rms radius becomes larger and the monopole matrix element becomes smaller. This indicates that the higher the excitation energy is, the more evolved the clustering is. The evolution of the clustering can be described by solving the Hill-Wheeler equation concerning the model parameters $\boldsymbol{\beta}_1$ and $\boldsymbol{\beta}_2$.

This respect is made much clearer by calculating the following squared overlap:

$$\mathcal{O}_\lambda(\boldsymbol{\beta}_1,\boldsymbol{\beta}_2) = \left|\langle\widetilde{\Phi}^{J=0}_\lambda(\boldsymbol{\beta}_1,\boldsymbol{\beta}_2)|\Psi_\lambda\rangle\right|^2, \tag{7}$$

with $\widetilde{\Phi}^{J=0}_\lambda(\boldsymbol{\beta}_1,\boldsymbol{\beta}_2)$ the normalized single eTHSR wave function in a space orthogonal to the lower eigenstates, i.e.,

$$\widetilde{\Phi}^{J=0}_\lambda(\boldsymbol{\beta}_1,\boldsymbol{\beta}_2) = \mathcal{N}_\lambda \widehat{P}_\lambda \Phi^{J=0}(\boldsymbol{\beta}_1,\boldsymbol{\beta}_2), \tag{8}$$

where $\widehat{P}_\lambda = 1 - \sum_{i=1}^{\lambda-1}|\Psi_i\rangle\langle\Psi_i|$ with $\lambda = I,\ldots,IV$, and $\widehat{P}_V = 1 - \sum_{i=1}^{6}|\Psi_i\rangle\langle\Psi_i|$, and $\mathcal{N}_\lambda$ are the corresponding normalization constants.

This quantity indicates how these five states Ψ_λ ($\lambda = I,\ldots,V$) are expressed by single configurations of the eTHSR wave functions, and therefore, gives direct information of whether the "container" structure is realized or not in these states, and if so, what kind of "containers" represent the states. In Fig. 3, the contour maps of the squared overlap of the states $\Psi_I - \Psi_V$ with single configurations in the $\beta_{2\perp}$ and β_{2z} parameter space in Eq. (7) are shown. Here the $\boldsymbol{\beta}_1$ parameter, i.e., $(\beta_{1\perp},\beta_{1z})$ is fixed at the position denoted by $\otimes$ in these figures, so that the maximum value of the squared overlap in the four parameter space $(\beta_{1\perp},\beta_{1z},\beta_{2\perp},\beta_{2z})$ appears at the position denoted by $\times$. The maximal values and $\boldsymbol{\beta}_1$ and $\boldsymbol{\beta}_2$ parameter values to give the maxima are listed in Table II. The corresponding $\boldsymbol{B}_1$ and $\boldsymbol{B}_2$ values are also shown.

Before discussing the features of the $0^+_I - 0^+_V$ states, I show in Table III the maximum values of the squared overlap of the 0^+_1, 2^+_1, and 0^+_2 states in ^{12}C with the single 3α THSR configuration. These are the same calculations as those for ^{16}O. The states in ^{12}C are calculated with the 3α THSR ansatz with the same F1 force parameters. It is now well known that these states are very precisely described by single THSR configurations, compared with the 3α RGM and 3α GCM [40], not only for the Hoyle state ($^{12}\mathrm{C}(0^+_2)$) but also for the other 0^+_1 and 2^+_1 states [19]. All these very large squared overlap values shown in this table again mean that the present "container" picture nicely holds not only for the dilute gaslike Hoyle state but also for the much more compact 0^+_1 and 2^+_1 states.

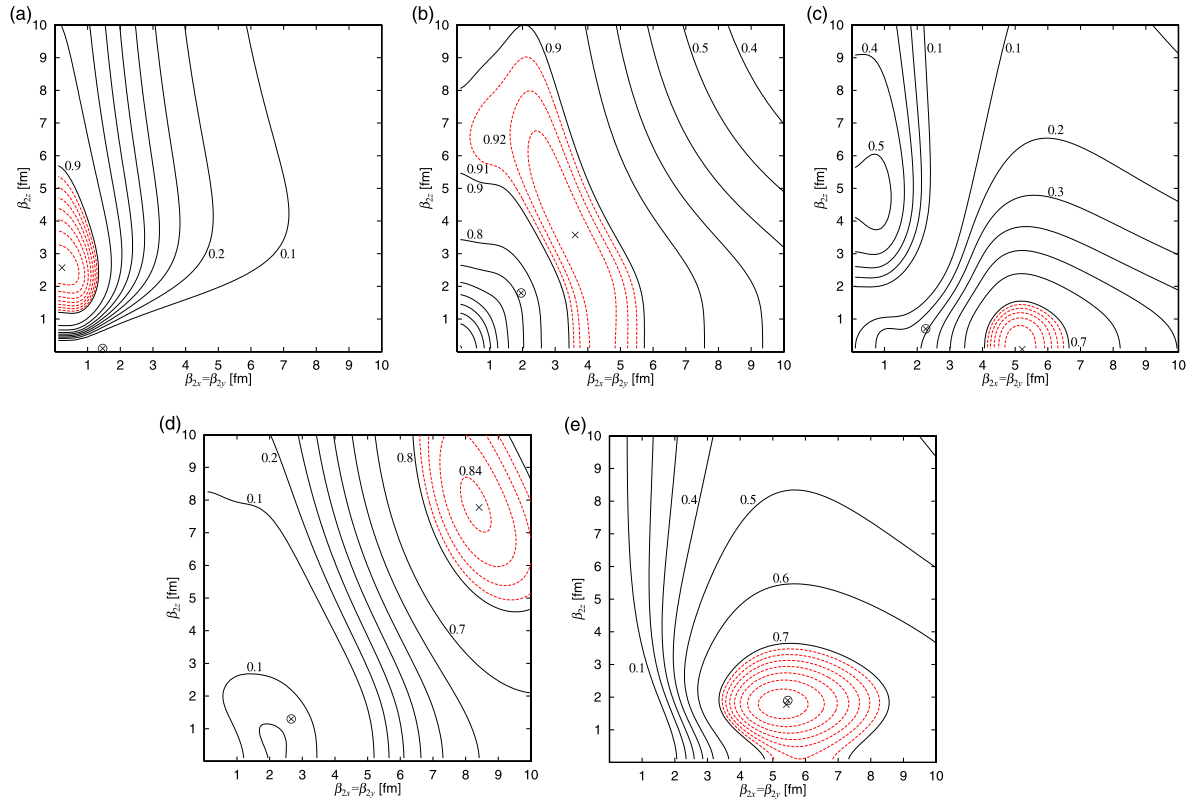

FIG. 3. Contour maps of the squared overlaps between the 0_I^+ (a), 0_{II}^+ (b), 0_{III}^+ (c), 0_{IV}^+ (d), and 0_V^+ (e) states, and the single extended deformed THSR wave functions, in two-parameter space $\beta_{2x} = \beta_{2y}$ and β_{2z}, in which $\boldsymbol{\beta}_1$ parameter values are fixed at optimal ones, denoted by $\otimes$, so that the maxima in four-parameter space $\beta_{1x} = \beta_{1y}$, β_{1z}, $\beta_{2x} = \beta_{2y}$, β_{2z} appear in these figures. The maximum positions are denoted by $\times$. Red dotted contour lines are in a step of 0.01 and black solid ones are in a step of 0.1.

Then, let us investigate the features for all these $0_I^+ - 0_V^+$ states one by one.

In the ground state, shown in Fig. 3(a), 3α clusters are put into an oblately deformed and very compact "container" with $\beta_{1\perp} \gg \beta_{1z}$, while the remaining α cluster is put into a prolately deformed and very compact "container" with $\beta_{2\perp} \ll \beta_{2z}$. This means that the first 3α clusters move in a xy plane and the last α cluster moves in the z direction. This supports the idea that the ground state has a tetrahedral shape of the 4α clusters proposed by several authors [41,42]. Our calculation indicates that this configuration is contained in the 0_I^+ state by 98%.

In the 0_{II}^+ state, shown in Fig. 3(b), the 3α clusters are in a spherical "container" with $\beta_{1\perp} \sim \beta_{1z}$. The fourth α cluster is put into a larger size "container" with spherical shape, i.e., $\beta_{2\perp} \sim \beta_{2z} > \beta_{1\perp} \sim \beta_{1z}$. In particular, the parameter set $(\beta_{1\perp},\beta_{1z}) = (1.8,1.8$ fm) is almost the same as that for ^{12}C in Table III, i.e., $(\beta_\perp,\beta_z) = (1,9,1.8$ fm). This means that the first 3α clusters are confined in a compact "container" to form the ground state of ^{12}C, because the $^{12}\mathrm{C}(0_1^+)$ state can be very precisely described by the single configuration with these parameter values. The fourth α cluster moves in a larger spherical "container" because of $(\beta_{2\perp},\beta_{2z}) = (3.5,3.6$ fm), which gives the largest squared overlap 94%. This is the new interpretation of the $\alpha + {}^{12}$C cluster structure, whose traditional understanding is that the α cluster orbits in an S wave around the $^{12}\mathrm{C}(0_1^+)$ state.

The 0_{III}^+ state, shown in Fig. 3(c), is similar to the 0_{II}^+ state but both "containers" are not spherical but deformed. The $\boldsymbol{\beta}_1$ parameter takes almost the same value as that of the isolated $^{12}\mathrm{C}(2^+)$ state, as shown in Table III, which means

TABLE II. Maxima of the squared overlaps in Fig. 3, for the $0_I^+ - 0_V^+$ states, in the four-parameter space $(\beta_{1\perp},\beta_{1z},\beta_{2\perp},\beta_{2z})$. The corresponding parameter values $(B_{1\perp},B_{1z},B_{2\perp},B_{2z})$ are also shown.

	$\mathcal{O}_{\max}$	$(\beta_{1\perp}, \beta_{1z}, \beta_{2\perp}\, \beta_{2z})$	$(B_{1\perp}, B_{1z}, B_{2\perp}, B_{2z})$
0_I^+	0.98	(1.3, 0.1, 0.1, 2.6 fm)	(2.3, 1.4, 1.4, 3.9 fm)
0_{II}^+	0.94	(1.8, 1.8, 3.5, 3.6 fm)	(2.9, 2.9, 5.2, 5.3 fm)
0_{III}^+	0.76	(2.1, 0.7, 5.1, 0.1 fm)	(3.3, 1.7, 7.4, 1.4 fm)
0_{IV}^+	0.84	(2.5, 1.3, 8.3, 7.8 fm)	(3.8, 2.3, 11.8, 11.1 fm)
0_{IV}^+	0.78	(5.3, 1.9, 5.3, 1.8 fm)	(7.6, 3.0, 7.6, 2.9 fm)

TABLE III. Maxima of the squared overlaps for the 0_1^+, 2_1^+, and 0_2^+ states in ^{12}C in two-parameter space $\beta_\perp$ and β_z. The corresponding $B_\perp$ and B_z values are also shown.

	$\mathcal{O}_{\max}$	$(\beta_\perp, \beta_z)$	$(B_\perp, B_z)$
$^{12}\mathrm{C}(0_1^+)$	0.93	(1.9, 1.8 fm)	(3.0, 2.9 fm)
$^{12}\mathrm{C}(2_1^+)$	0.90	(1.9, 0.5 fm)	(3.0, 1.6 fm)
$^{12}\mathrm{C}(0_2^+)$	0.99	(5.6, 1.4 fm)	(8.0, 2.4 fm)

that the first 3α clusters form the $^{12}C(2^+)$ state, because the state is described by the single parameter value of $\boldsymbol{\beta}$. The configuration of the remaining α cluster $(\beta_{2\perp},\beta_{2z}) =$ (5.1,0.1 fm), giving the largest value 76%, means that the α cluster moves in a deformed and larger "container." This is the present understanding of the 0_3^+ state, which is conventionally considered to have the $\alpha(D) + {}^{12}C(2^+)$ structure.

In the 0_{IV}^+ state, shown in Fig. 3(d), one can see that the 3α clusters are put in a slightly larger "container" than that for the $^{12}C(0_1^+)$ state, which is slightly deformed in an oblate shape. The fourth α cluster, however, moves in a much larger and almost spherical "container," like a satellite. This configuration expresses the 0_{IV}^+ state dominantly by 84%. This means that the second "container" characterized by $\boldsymbol{\beta}_2$ is further evolved from that in the 0_{II}^+ state. I can say that this state corresponds to the 0_4^+ state in the former 4α OCM calculation, which predicts the $\alpha + {}^{12}C(0_1^+)$ higher nodal structure for the state.

The 0_V^+ state, shown in Fig. 3(e), is the most striking. All the α clusters occupy an identical orbit, with $(\beta_{1\perp},\beta_{1z},\beta_{2\perp},\beta_{2z}) =$ (5.3, 1.9, 5.3, 1.8 fm). This is qualified to call the α condensation. This configuration is contained in this state by 78%, which is still very large. Furthermore, this "container" is very close to the one of the Hoyle state, with $(\beta_{1\perp},\beta_{1z}) =$ (5.6, 1.4 fm) in Table III. This means that the 0_V^+ state is regarded as the Hoyle analog state, in which the fourth α cluster is also put into the "container" occupied with the 3α clusters in the Hoyle state. The large size of this "container" indicates that the 4α clusters are loosely coupled with each other and configured like a gas. Note that the 4α condensate state is also predicted by the 4α OCM calculation slightly above the 4α threshold, as the 0_6^+ state.

These results tell us that the evolution of cluster structures is described by the "container" evolution with respect to its size and shape. The reason why the "container" evolution arises is the orthogonality to the lower states, which is explicitly taken into account in the definition of the single configuration $\widetilde{\Phi}_k^{J=0}$ in Eq. (7). The orthogonality condition prevents a higher state configuration from overlapping with the lower states' more compact configurations. It thus plays a role as a repulsive core and is considered to give the "container" evolution.

In conclusion, I introduced the eTHSR wave function, which comprehensively describes gaslike and non-gaslike cluster states in ^{16}O, standing on the "container" picture. The evolution of the clustering, as the excitation energy increases, can be obtained by solving the Hill-Wheeler equation, concerning the "container" parameters. I showed that the evolution of the clustering is caused by the evolution of the "container." Not only various $\alpha + {}^{12}C$ cluster states but also the 4α gaslike state are naturally described according to this picture, in which the α clusters are confined into different size and shape "containers." In particular, the 4α gaslike state is obtained as having the same "container" for the 4α clusters, clearly giving the 4α condensate structure. This picture of "container" evolution is thus a key concept in heavier nuclei, to understand the dynamical process of formation of cluster structures, from the ground state to higher excited states.

The author wishes to thank B. Zhou, H. Horiuchi, A. Tohsaki, G. Röpke, P. Schuck, and T. Yamada for many fruitful discussions. This work is financially supported by the startup fund for the associate professorship of "Zhuoyue 100" program, Beihang University.

[1] K. Ikeda, H. Horiuchi, and S. Saito, Suppl. Prog. Theor. Phys. **68**, 1 (1980).
[2] T. K. Rana *et al.*, Phys. Rev. C **88**, 021601(R) (2013).
[3] M. Freer and H. O. U. Fynbo, Prog. Part. Nucl. Phys. **78**, 1 (2014), and references therein.
[4] M. Itoh *et al.*, Phys. Rev. Lett. **113**, 102501 (2014).
[5] A. Tohsaki, H. Horiuchi, P. Schuck, and G. Röpke, Phys. Rev. Lett. **87**, 192501 (2001).
[6] Y. Funaki, A. Tohsaki, H. Horiuchi, P. Schuck, and G. Röpke, Phys. Rev. C **67**, 051306(R) (2003).
[7] T. Yamada and P. Schuck, Phys. Rev. C **69**, 024309 (2004).
[8] T. Yamada and P. Schuck, Eur. Phys. J. A **26**, 185 (2005).
[9] Y. Funaki, T. Yamada, H. Horiuchi, G. Röpke, P. Schuck, and A. Tohsaki, Phys. Rev. Lett. **101**, 082502 (2008).
[10] Y. Funaki, H. Horiuchi, and A. Tohsaki, Prog. Part. Nucl. Phys. **82**, 78 (2015).
[11] B. Zhou, Z. Z. Ren, C. Xu, Y. Funaki, T. Yamada, A. Tohsaki, H. Horiuchi, P. Schuck, and G. Röpke, Phys. Rev. C **86**, 014301 (2012); B. Zhou, Y. Funaki, H. Horiuchi, Z. Z. Ren, G. Röpke, P. Schuck, A. Tohsaki, C. Xu, and T. Yamada, Phys. Rev. Lett. **110**, 262501 (2013); Phys. Rev. C **89**, 034319 (2014).
[12] T. Suhara, Y. Funaki, B. Zhou, H. Horiuchi, and A. Tohsaki, Phys. Rev. Lett. **112**, 062501 (2014).
[13] H. Morinaga, Phys. Rev. **101**, 254 (1956); Phys. Lett. **21**, 78 (1966).
[14] T. Yamada, Y. Funaki, H. Horiuchi, K. Ikeda, and A. Tohsaki, Prog. Theor. Phys. **120**, 1139 (2008); T. Yamada, Y. Funaki, T. Myo, H. Horiuchi, K. Ikeda, G. Röpke, P. Schuck, and A. Tohsaki, Phys. Rev. C **85**, 034315 (2012).
[15] M. Freer, H. Horiuchi, Y. Kanada-En'yo, D. Lee, and U.-G. Meißner, arXiv:1705.6192.
[16] B. Zhou, Y. Funaki, H. Horiuchi, and A. Tohsaki (unpublished).
[17] K. Ikeda, N. Takigawa, and H. Horiuchi, Suppl. Prog. Theor. Phys. **E68**, 464 (1968).
[18] Y. Funaki, H. Horiuchi, A. Tohsaki, P. Schuck, and G. Röpke, Prog. Theor. Phys. **108**, 297 (2002).
[19] Y. Funaki, A. Tohsaki, H. Horiuchi, P. Schuck, and G. Röpke, Eur. Phys. J. A **24**, 321 (2005); **28**, 259 (2006).
[20] B. Zhou, Y. Funaki, A. Tohsaki, H. Horiuchi, and Z. Z. Ren, Prog. Theor. Exp. Phys. **2014**, 101D01 (2014).
[21] Y. Funaki, Phys. Rev. C **92**, 021302(R) (2015); **94**, 024344 (2016).
[22] B. Zhou, A. Tohsaki, H. Horiuchi, and Z. Z. Ren, Phys. Rev. C **94**, 044319 (2016).
[23] Y. Funaki, T. Yamada, A. Tohsaki, H. Horiuchi, G. Röpke, and P. Schuck, Phys. Rev. C **82**, 024312 (2010).

[24] M. Lyu, Z. Z. Ren, B. Zhou, Y. Funaki, H. Horiuchi, G. Röpke, P. Schuck, A. Tohsaki, C. Xu, and T. Yamada, Phys. Rev. C **91**, 014313 (2015).
[25] M. Lyu, Z. Z. Ren, B. Zhou, Y. Funaki, H. Horiuchi, G. Röpke, P. Schuck, A. Tohsaki, C. Xu, and T. Yamada, Phys. Rev. C **93**, 054308 (2016).
[26] Y. Funaki, T. Yamada, E. Hiyama, B. Zhou, and K. Ikeda, Prog. Theor. Exp. Phys. **2014**, 113D01 (2014).
[27] Y. Funaki, M. Isaka, E. Hiyama, T. Yamada, and K. Ikeda, Phys. Lett. B **773**, 336 (2017).
[28] Y. Funaki, H. Horiuchi, W. von Oertzen, G. Röpke, P. Schuck, A. Tohsaki, and T. Yamada, Phys. Rev. C **80**, 064326 (2009).
[29] D. M. Brink, in *Proceedings of the International School of Physics Enrico Ferm, Course 36, Varenna*, edited by C. Bloch (Academic Press, New York, 1966).
[30] Y. Kanada-En'yo, H. Horiuchi, and A. Ono, Phys. Rev. C **52**, 628 (1995); Y. Kanada-En'yo and H. Horiuchi, *ibid.* **52**, 647 (1995).
[31] Y. Funaki, H. Horiuchi, and A. Tohsaki, Prog. Theor. Phys. **115**, 115 (2006).
[32] A. Tohsaki, Phys. Rev. C **49**, 1814 (1994).
[33] A. B. Volkov, Nucl. Phys. A **74**, 33 (1965).
[34] N. Itagaki, A. Ohnishi, and K. Katō, Prog. Theor. Phys. **94**, 1019 (1995).
[35] N. Itagaki, Phys. Rev. C **94**, 064324 (2016).
[36] Y. Suzuki, Prog. Theor. Phys. **55**, 1751 (1976); **56**, 111 (1976).
[37] K. Fukatsu and K. Katō, Prog. Theor. Phys. **87**, 151 (1992).
[38] F. Ajzenberg-Selove, Nucl. Phys. A **460**, 1 (1986).
[39] T. Wakasa *et al.*, Phys. Lett. B **653**, 173 (2007).
[40] Y. Fujiwara, H. Horiuchi, K. Ikeda, M. Kamimura, K. Katō, Y. Suzuki, and E. Uegaki, Suppl. Prog. Theor. Phys. **68**, 29 (1980).
[41] R. Bijker and F. Iachello, Phys. Rev. Lett. **112**, 152501 (2014).
[42] Y. Kanada-En'yo, Phys. Rev. C **96**, 034306 (2017).